Manifold of spin states and dynamical temperature effects in LaCoO_{3}: Experimental and theoretical insights

M. Feygenson, D. Novoselov, S. Pascarelli, R. Chernikov, O. Zaharko, F. Porcher, D. Karpinsky, A. Nikitin, D. Prabhakaran, A. Sazonov, and V. Sikolenko

Phys. Rev. B **100**, 054306 — Published 28 August 2019

DOI: 10.1103/PhysRevB.100.054306

Manifold of spin-states and dynamical temperature effects in $LaCoO_3$: experimental and theoretical insights

M. Feygenson,[1] D. Novoselov[2,3], S. Pascarelli,[4] R. Chernikov,[5]O. Zaharko,[6]F. Porcher,[7] D. Karpinsky,[8]A. Nikitin,[8] D. Prabhakaran,[9] A. Sazonov,[10]V. Sikolenko,[11,*]

[1]*Forschungszentrum Jülich, JCNS-1, D-52425 Jülich, Germany*

[2]*M.N. Mikheev Institute of Metal Physics,*

Ural Branch of the Russian Academy of Sciences,

18 S. Kovalevskaya Street, Yekaterinburg, 620108 Russia

[3]*Ural Federal University, 19 Mira Street, Yekaterinburg, 620002, Russia*

[4]*European Synchrotron Radiation Facility, BP 220, 38043 Grenoble, France*

[5]*Canadian Light Source, 44 Innovation Boulevard, Saskatoon SK S7N 2V3, Canada*

[6] *Laboratory for Neutron Scattering and Imaging,*

Paul Scherrer Institute, CH-5232 Villigen PSI, Switzerland

[7]*CEA Saclay Laboratoire Lèon Brillouin F-91191 Gif Sur Yvette, France*

[8]*Scientific-Practical Materials Research Centre of NAS of Belarus, 220072 Minsk, Belarus*

[9]*Clarendon Laboratory, Parks Road,*

Oxford OX1 3PU, United Kingdom

[10]*European Spallation Source (ESS) ERIC,*

Data Management and Software Centre (DMSC), 2200 Copenhagen, Denmark and

[11]*Joint Institute for Nuclear Research,*

*Joliot-Curie 6, 141980 Dubna, Russia**

(Dated: June 19, 2019)

Abstract

The unconventional transport and magnetic properties of perovskite-like lanthanum cobalt oxide $LaCoO_3$ have been studied for more than five decades. This highly correlated-electron system exhibits a variety of peculiar properties that are desirable for environmentally-friendly energy solutions, fuel cell technologies, novel diesel engines and oxyfuel power plants. However, the true spin-state of Co^{3+} ion is an important but still unresolved issue that underlies those applications. Although many theoretical models were proposed, finding supporting experimental evidences of spin-state transitions is extremely difficult. It is not until recently, that new advanced scattering methods have emerged allowing unprecedented precision in determining the crystal structure of $LaCoO_3$. In this work, we combined high-resolution extended x-ray absorption fine structure, x-ray powder diffraction, neutron powder and single crystal diffraction over a broad range of temperatures from 2 up to 1000 K, as well as quantum mechanical modeling to study the spin-state transition in $LaCoO_3$ and in a reference sample of $LaGaO_3$. Our results suggested that the Co ions are mainly in a low-spin state at temperatures below 150 K, with a minority of ions in the high-spin state. With an increase of the temperature the gradual transition from low to intermediate-spin state occurs up until 550 K. At the metal-insulator transition at 550 K, the long-range domains of the intermediate-spin states have become a dominant contribution. Above 550 K, the transition from intermediate- to high-spin state was observed. It was established that a slight change in the degree of pd-hybridization can lead to the appearance of a spin-state transition which might be induced by both temperature and surface effects in powder crystallites.

**To whom correspondence should be addressed:sikolen@jinr.ru

I. INTRODUCTION

Perovskite-like lanthanum cobalt oxide $LaCoO_3$ is a fascinating material studied since 1950s due to its unconventional structural [1–7], transport [8–11] and magnetic [11–14] properties, explanation of which still remains controversial. There is a peak at 120 K for both magnetic susceptibility and thermal expansion coefficient of $LaCoO_3$, followed by a plateau at 550 K associated with the metal-insulator transition [8, 11, 13]. Goodenough et al. [15, 16] proposed that both transitions are of magnetic origin related to spin-state transitions of Co^{3+} ions from the nonmagnetic low-spin (LS; $t_{2g}^6 e_g^0$, S = 0) to a high-spin (HS; $t_{2g}^4 e_g^2$, S = 2) state. Such transitions are result of comparable values of the intra-atomic exchange energy (J_H) and crystal field splitting (10Dq) at the Co^{3+} sites. Thus, depending on the relative values of J_H and 10Dq, either LS or HS state could become more stable. The LS−HS model assumes that the population of LS and HS states is temperature dependent and coexistence of both LS and HS states is possible in the temperature range of 120 − 550 K [9, 17–26]. The alternative scenario of the spin-state transitions was proposed in 1995. Potze et al [27] introduced the concept of an intermediate-spin state (IS; $t_{2g}^5 e_g^1$, S = 1) and showed that the spin-state transition near 120 K could be associated with the thermal excitation of Co^{3+} ions from the LS ground state to IS state, whereas the second transition at 550 K corresponds to a crossover from the IS state to a mixture of IS and HS states [27, 28]. The existence of Co^{3+} in HS above 500 K was experimentally confirmed by electro-conductivity, photoemission, thermal expansion and specific heat capacity measurements [12, 27, 28]. Additional evidence of the IS state was provided by local density approximation (LDA+U) band structure calculations assuming that the temperature effects and spin-state transitions can be simulated by expanding the lattice parameter [29]. According to Korotin et al [29], the stabilization of the IS state is due to a large pd-hybridization between the Co 3d (e_g) and O 2p levels. The partially filled e_g level makes the IS state Jahn−Teller (JT) active. The degeneracy of the e_g orbitals of Co^{3+} ions in the LS state is expected to be lifted in the IS state by a JT distortion which is not compatible with the $R\bar{3}c$ (D_{3d}^6) symmetry [1]. Therefore, the LS−IS scenario has become widely used in interpretation of experimental results [2–4, 12, 30]. Clearly, the issue of the true spin states of the Co^{3+} ions between 120 K and 550 K in $LaCoO_3$ still remains unresolved.

In this work, we are addressing this issue by combining EXAFS and diffraction studies of the temperature dependence of Co−O bond length for T=2−1000 K. For those studies, we also used a powder sample of $LaGaO_3$ with Ga^{3+} in the LS state as a reference to carefully distinguish between contributions of different spin states. The dynamical mean-field theory (DFT+DMFT) approach [31–34] was used for studies of the spin-state transition dependence on ionic radii of cobalt in $LaCoO_3$. The influence of the relative position of O-p and Co-d levels on the transition process was also studied, taking into account the temperature dynamical effects and strong electron correlations. Our measurements and theoretical calculations revealed an importance of IS states and provided a consistent model of the spin-state transitions in $LaCoO_3$ over a broad temperature range.

II. METHODS

A. Sample preparation

The single-crystal of $LaCoO_3$ was grown by the floating-zone technique in an image furnace under high pressure. The detailed synthesis and characterization measurements of $LaCoO_3$ single crystal are described elsewhere [35]. The powder sample was obtained by subsequently crushing this single-crystal. The powder for synchrotron x-ray diffraction was grounded and run through a sieve, while powder for neutron diffraction was only grounded.

B. Extended x-ray absorption fine structure measurements

The extended x-ray absorption fine structure (EXAFS) experiments have been performed at the beamline BM29 at European Synchrotron Radiation Facility, France. The storage ring energy and average current were 6.0 GeV and 200 mA, respectively. The EXAFS spectra were measured in the temperature range from 12 K up to 650 K in the energy range 7400−9500 eV in standard transmission mode simultaneously with a reference sample using three ionization chambers filled with argon gas. X-ray absorption spectra above the Ga K-edge (10367 eV) were measured in the temperature range from 10 K up to 900 K in transmission mode at the beamline BL01B1 at Spring-8 Synchrotron, Japan. EXAFS spectra were treated using the EDA software package following the standard procedure

[36]. The energy position E_0, used in the definition of the photoelectron wave number $k = [(2me/\hbar^2)(E - E_0)]^{1/2}$, was set at the threshold energy E_0 = 7714 eV.

C. Neutron and x-ray scattering measurements

The single-crystal neutron diffraction experiments were carried out in the temperature range from 3 K to 750 K on the neutron diffractometers TRICS (Paul Scherrer Institut, Switzerland) using λ = 1.18 Å and RESI (Heinz Maier-Leibnitz Zentrum, Germany) using a wavelength of 1.0 Å. For most temperature points we collected all the accessible reflections with a $\sin\theta/\lambda$ range up to 0.85 Å^{-1}.

The neutron powder diffraction (NPD) experiments were carried out at 3T2 beamline at Laboratoire Lèon Brillouin, France. The data was collected at λ = 1.23 Å over 2θ of 4.5121^o at various temperatures from 2 K to 1000 K.

The synchrotron x-ray powder (XPD) measurements were performed on BM01 diffractometer at ESRF on the KUMA6 diffractometer at the wavelength of λ = 0.65 Å with a $\sin\theta/\lambda$ range 1.0 Å^{-1} in the temperature range from 80 K up to 700 K. Additional measurements were carried out at 11BM beamline at Advanced Photon Source in Argonne National Laboratory, USA with λ = 0.4145 Å with a $\sin\theta/\lambda$ range 1.1 Å^{-1}, in the temperature range of 9 K to 1000 K.

D. Calculation methods

The density functional theory (DFT) part was calculated in the generalized gradient approximation by the plane wave method implemented in the Quantum-Espresso package [37]. The dynamic mean field theory (DMFT) calculations were carried out by the AMULET package (amulet.org) with the state-of-the-art continuous-time quantum Monte-Carlo (CT-QMC) solver [38–41] applied to all five 3d-orbitals of the Co ion. The Hubbard U=6 eV and Hund's coupling J=0.8 eV were used [42, 43]. The crystal structure data obtained from the experiment at the temperatures T = 20, 300 and 700 K were used as a starting point for the DFT calculations. The Hamiltonians including d-Co and p-O states were constructed by using the Wannier functions and which have been used as initial data for the DMFT

calculations. In the spin-state transition temperature range from 20 to 700 K, the interval for the Δ_{p-d} value from 0.6 to 1.2 eV was considered as a physically relevant and the value of 0.6 eV was taken for the calculations. The value of the statistical weight of IS d^6 state was 0.1 eV, which remained constant during the changing both temperature and Δ_{p-d}. Due to the fact that $LaCoO_3$ compound may be treated as a charge-transfer [44, 45], one can assume that $d^7\underline{L}$ states have the effective total spin S_{tot}=1 (IS) or S_{tot}=0 (LS). The superposition of the states with S=1 may has the weight comparable with the contributions with S=0 and S=2 states and even slightly exceed each of them separately in a narrow vicinity of the crossover. The hybridization between p-states of the ligands and d-states of the ions decreases when moving from the core of the crystallite to its surface, and the relative distance between the centers of mass of the corresponding zones also changes. When Δ_{p-d} parameter is varied, the region of the spin-state transition for a given temperature is rather narrow (less than 0.1 eV) as compared with the interval between the temperature spin-state transitions (about 0.6 eV). Thus, depending on the penetration depth in the crystallite, the surface spin states might be different from the states dominating in the core of the crystallite (including S=1 states), even at the same temperature.

E. Parameters

In this section we outline the definitions of parameters derived from the refinements of the experimental data. $MSRD_{||}$ is the parallel mean square relative displacement for Co-O and Ga-O bonds obtained from EXAFS data analysis. The mean square displacement (MSD) was obtained from x-ray and neutron diffraction data. It describes displacement of atoms from their mean position. The difference between uncorrelated MSD obtained by diffraction and correlated $MSRD_{||}$ obtained by EXAFS is defined as the displacement correlation function (DCF). The DCF describes the correlation in the atomic motion of Co/Ga and O atoms and defines the strength of the corresponding bond. The isotropic atomic displacement parameter (ADP) was obtained from powder diffraction data for Co and O atoms. The oxygen displacement parameters parallel ($U_{||}$) and perpendicular ($U_{\perp}$) to the Co−O bond were obtained from the analysis of the single-crystal neutron diffraction data.

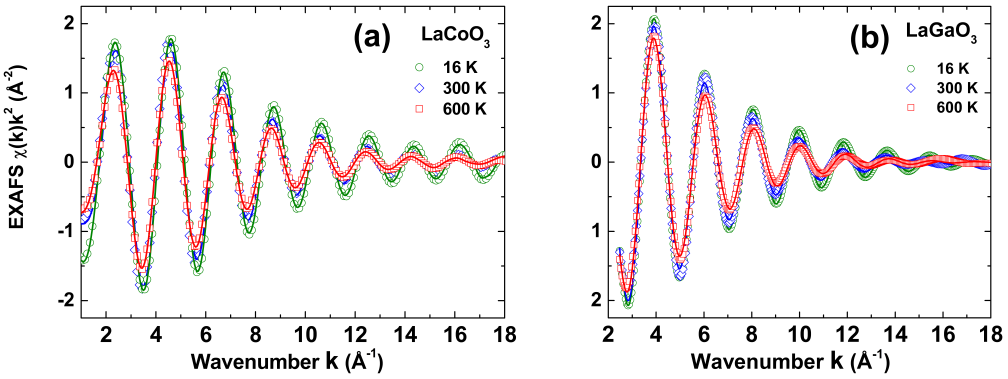

FIG. 1: Experimental (open symbols) and calculated (solid lines) EXAFS signals $\chi(k)k^2$ at Co and Ga K-edges at different temperatures for (a) $LaCoO_3$ and (b) $LaGaO_3$ samples.

III. RESULTS

The EXAFS data were analyzed using the procedure described in Ref.[46]. The averaged Co−O and Ga−O bond lengths and $MSRD_{||}$ within the first coordination shell were determined for $LaCoO_3$ and $LaGaO_3$ samples. The experimental scattering amplitude and phase shift functions for the Co−O atomic pair were used in the EXAFS analysis. They were obtained from the EXAFS spectra of the powdered $LaCoO_3$ sample, measured at T = 16 K, with the assumption of regular CoO_6 octahedra with no significant anharmonicity in dynamics. Moreover, the cobalt coordination number $N_{ref} = 6$ and Co−O distance $R_{ref} = 1.925$ Å were set according to the results of the Rietveld refinement of our x-ray powder diffraction data of $LaCoO_3$. The high-resolution EXAFS $\chi(k)k^2$ spectra with a high signal to noise ratio up to high momentum transfer of $2k_{max} = 36$ Å^{-1} from the first coordination shell for $LaCoO_3$ and $LaGaO_3$ at 16 K, 300 K and 600 K are shown in Fig. 1.

The neutron and synchrotron x-ray diffraction experiments were carried out for $LaCoO_3$ and $LaGaO_3$ powders. Additional neutron scattering studies of the high-quality single crystal of $LaCoO_3$ were carried out as well. The combination of x-ray and neutron scattering methods allowed us to carefully refine atomic positions and displacement parameters across spin-state transitions. Neutrons are sensitive to light elements; thus, the position of the O atoms is more accurately determined than with x-ray scattering. Complimentary x-ray scattering measurements were used to verify the neutron scattering results and provide an independent probe for La and Co atomic positions. The combined Rietveld refinements were

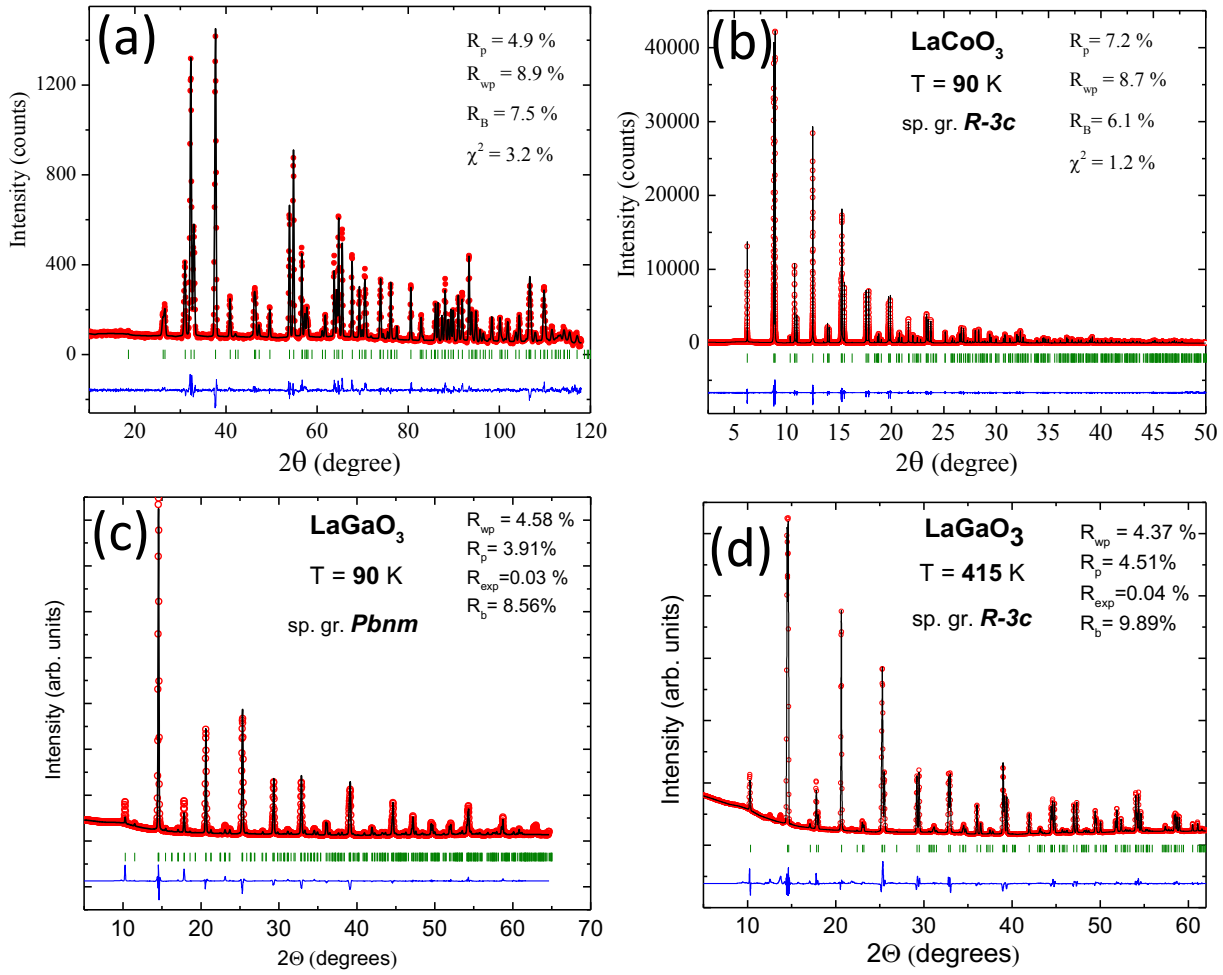

FIG. 2: (a) (Color online) NPD pattern of $LaCoO_3$ at 10 K, (b) Rietveld refinement of X-ray powder diffraction pattern of $LaGaO_3$ at 90 K (11BM beamline at APS). Rietveld refinement of X-ray powder diffraction patterns (BM-01, ESRF) measured for $LaGaO_3$ at (a) 90 K and (b) 415 K. The experimental data (open circles), refinement (solid line) and difference curve (solid line at the bottom). The tick marks indicate the calculated positions of the Bragg peaks.

performed using FULLPROF [47]. The representative refinements of neutron and x-ray data are shown in Fig. 2 and results are outlined in Table I.

From Rietveld refinements of the powder samples, we derived the temperature dependence of the following parameters : Co-O bond length, isotropic ADP for Co^{3+} ions and strain parameter. The anisotropic ADP of oxygen were obtained from the refinements of the neutron single-crystal $LaCoO_3$ diffraction data and consequentially the oxygen displacement parameters parallel ($U_{||}$) and perpendicular ($U_{\perp}$) to the Co−O bond across the spin-state and metal-insulator transitions were revealed. The results of refinements are

TABLE I: Details of Rietveld refinements presented in Fig.2.

Rietveld								
$LaCoO_3$ (10 K), NPD					**$LaCoO_3$ (90 K), XPD**			
Space group	R-3c				R-3c			
a,b,c (Å)	5.421043	5.421043	12.979095		5.427989	5.427989	13.009775	
Atom	x	y	z	Occ.	x	y	z	Occ.
La1	0.00000	0.00000	0.25000	0.16666	0.00000	0.00000	0.25000	1.00000
Co1	0.00000	0.00000	0.00000	0.16666	0.00000	0.00000	0.00000	1.00000
O1	0.55283	0.00000	0.25000	0.50401	0.55272	0.00000	0.25000	3.00268
$LaGaO_3$ (90 K), XPD					**$LaGaO_3$ (415 K), XPD**			
Space group	Pbnm				R-3c			
a,b,c (Å)	5.517093	5.488082	7.767441		5.532593	5.532593	13.379971	
Atom	x	y	z	Occ.	x	y	z	Occ.
La1	-0.00336	0.01941	0.25000	0.45041	0.00000	0.00000	0.25000	0.16500
Ga1	0.50000	0.00000	0.00000	0.54959	0.00000	0.00000	0.00000	0.16500
O1	0.06290	0.49871	0.25000	0.49904	0.44444	0.00000	0.25000	0.50959
O2	0.72337	0.26862	0.03463	0.99904				

summarized in Fig.3 and Fig. 4.

Fig.3a shows the temperature dependence of Co−O bond lengths obtained from the refinements of the EXAFS, x-ray and neutron powder diffraction data of $LaCoO_3$ sample. We note that the inter atomic distance $< r_{Co-O} > = < |r_O - r_{Co}| >$ probed by EXAFS is usually larger than the equilibrium crystallographic distance between average positions $R_{Co-O} = |< r_O > - < r_{Co} >|$ measured by diffraction [36, 49, 50, 58]. It is due to the thermal atomic displacement in the direction perpendicular to the Co−O bond $< \sigma^2_{\perp,Co-O} >$[49, 50]:

$$< r_{Co-O} >= R_{Co-O} + \frac{\sigma^2_{\perp,Co-O}}{2R_{Co-O}} \quad (1)$$

Surprisingly, the Co−O bond lengths in $LaCoO_3$ determined from the EXAFS analysis are gradually shorter as temperature increases with respect to the ones obtained from the diffraction experiments, up to a maximum difference around the metal-insulator transition temperature, T_{MI} = 550 K (Fig.3a).

Fig.3b shows oxygen displacement parameters $U_{||}$ and $U_{\perp}$ in Co−O−Co chain extracted from the single-crystal neutron diffraction data. $U_{\perp}$ and $U_{||}$ of oxygen in the single crystal

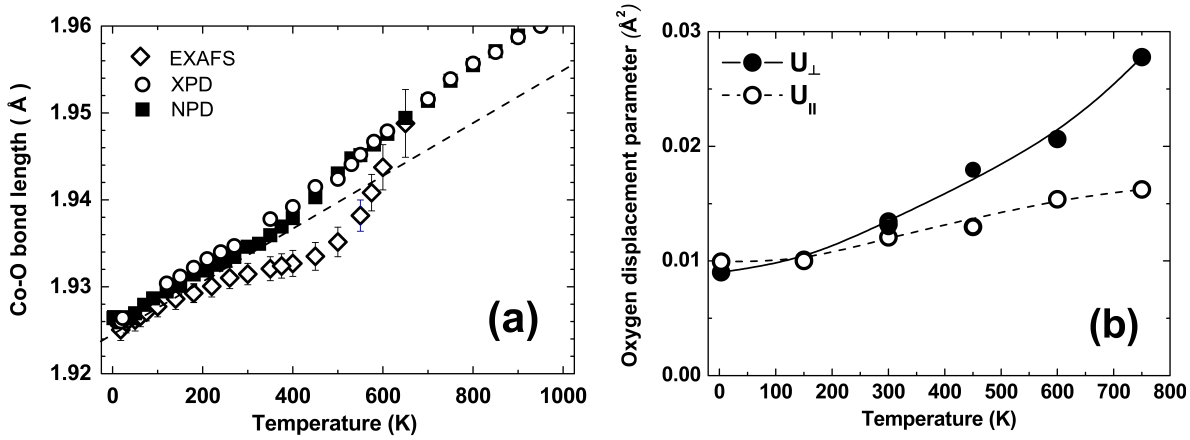

FIG. 3: (a) The temperature dependence of the Co−O bond length for $LaCoO_3$ (a) obtained by refinements of the EXAFS ($< r_{Co-O} >$), XPD and NPD data (R_{Co-O}). Dashed line shows a low-temperature linear slope for the reference. (b) Temperature dependence of $U_\perp$ and $U_{||}$ of oxygen for the $LaCoO_3$ single crystal.

of $LaCoO_3$ both increase with temperature, with $U_{||}$ showing an increase of about 50 % from the lowest to the highest temperature, while $U_\perp$ showing much steeper increase of about 300 %. The strain parameter obtained from XPD shows a broad peak at about 50 K and deviation from the linear behavior at temperatures above 550 K (Fig.4a). Moreover, the slope change of the isotropic ADP for Co at 50 K and 550 K was observed (Fig.4b). We note that measurements of the reference $LaGaO_3$ powder under the same experimental conditions showed neither of those effects.

The role of the finite size crystallites in the spin-state transitions in $LaCoO_3$ is often neglected during the analysis of the powder diffraction data, despite numerous reports on strain induced transitions in the thin films [51–56] and nanoparticles of $LaCoO_3$ [57]. The reduced dimensions of thin films and nanoparticles lead to a significant amount of strain, which directly affects the crystal structure of cobaltites. The finite-size effects are most pronounced in nanoscaled materials, however they have to be considered as well in our powders. In order to emphasize an important role of finite crystallites in the spin-state transitions, we carried out scanning electron transmission (SEM) measurements. Two separate powders used in x-ray and neutron powder diffraction were examined (Fig.5). The sample for synchrotron x-ray diffraction was grounded and run through a sieve with 10 μm

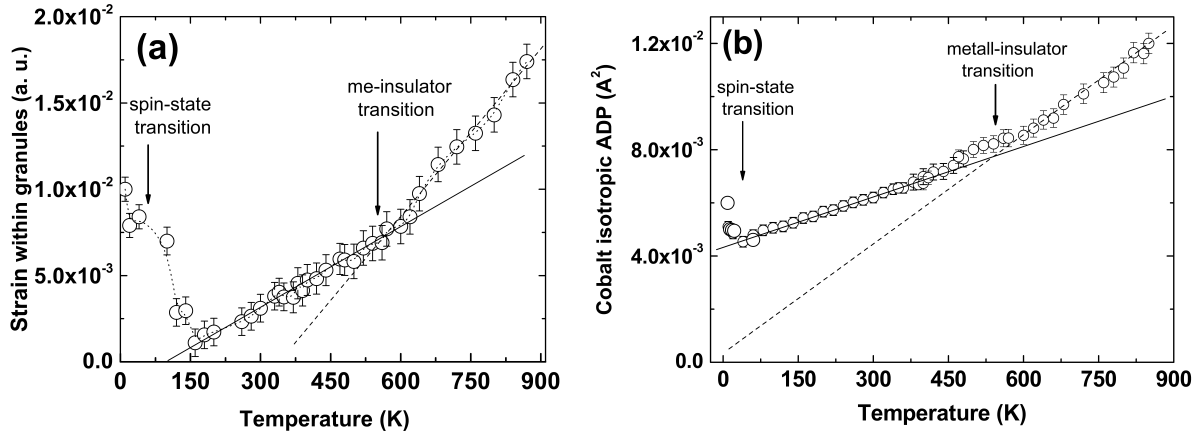

FIG. 4: (a) Temperature dependence of strains within crystallites obtained by the Rietveld analysis of XPD data. Dashed line is guide for the eye. (b) The isotropic ADP of Co in $LaCoO_3$ sample. The solid and dashed lines are the linear fits to the data above and below 550 K.

pore size. Such treatment resulted in the finite crystallites with overall sizes below 10 μm, evident in Fig.5a. For neutron scattering experiments the sample was only grounded and no sieve was used. As a result, crystallites and aggregates exceeding 10 μm were found in SEM studies (Fig.5b). The size distribution of crystallites in x-ray samples is narrower than in the samples prepared for neutron scattering measurements, hence the effect of strain is still visible in neutron data, but it is more pronounced in x-ray data. The size narrowing of the crystallites for two independent scattering experiments provided an excellent illustration of the role of the crystallites in our samples. On the other end of the spectrum, diffraction measurements of the bulk single-crystal were used as a reference of the sample possessing no finite crystallites. Therefore, no surface effects on the spin-state transitions are expected in the single-crystal of $LaCoO_3$.

It is important to note that an accurate description of dynamical and static properties of oxygen atom in our powder and single-crystal samples was possible by combining high-resolution x-ray and neutron scattering techniques. X-ray scattering is sensitive to the position of heavy Co atoms, while light O atoms provide much better contrast for neutron scattering. As a result, the positions and atomic displacements of both Co and O atoms were experimentally defined in a wide temperature range with a very high precision. Moreover, our diffraction combined with EXAFS studies provided unprecedented insights

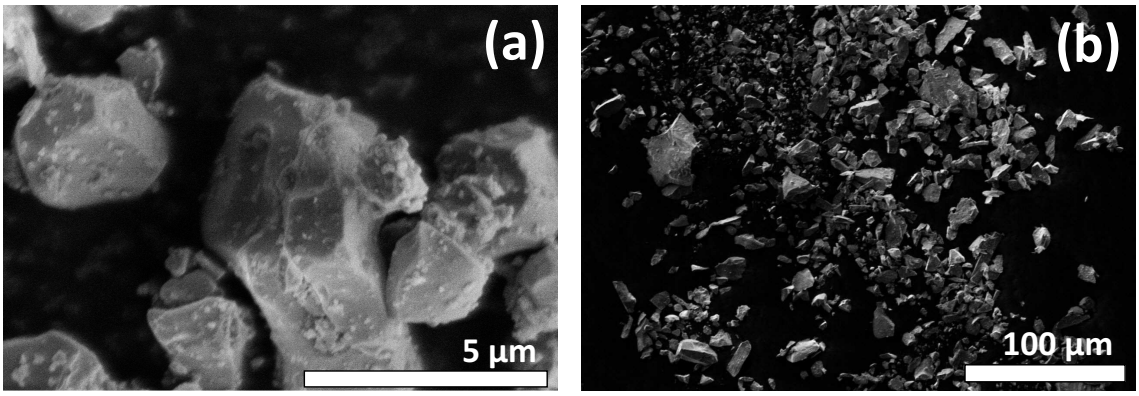

FIG. 5: The represenataive SEM images of $LaCoO_3$ powder used in (a) x-ray and (b) neutron scattering measurements.

into oxygen fluctuations by means of temperature-dependent DCF. Moreover, our results are in agreement with our previous findings of oxygen displacement parameters (parallel and perpendicular to the Co-O bond) increase with the temperature in $LaCoO_3$ single crystal. Such behavior was correlated with the softening of the TO_2 and hardening of TO_1 phonon branches along the $[0\ \xi\ \xi]$ high symmetry direction [48]

A combination of DFT and DMFT was used to quantitatively explain the experimental data. We note that the use of DFT alone is not sufficient to describe complex phase transitions in our samples. It is well known that DFT underestimates the electron-electron correlations for materials with a partially filled d-band and hence, it cannot properly describe the paramagnetic phase in $LaCoO_3$. The DFT+U method can take into account the electron-electron correlations, however it fails to describe the metal-insulator transition that accompanies the spin transition in $LaCoO_3$. Thus, the DFT+DMFT modeling allows to properly describe the characteristic properties of the $LaCoO_3$ system, i.e : (i) strong Coulomb correlations between electrons in partially filled d^3-Co states and (ii) transition from the paramagnetic into insulator phase, with increasing temperature. In addition, we used the CT-QMC algorithm to observe a complete statistical picture of the atomic states of the impurity in question (d−states of the Co atom), including multiplet configurations, and to observe its changes as a function of temperature, structure and degree of hybridization of 3d−Co and 2p−O states.

The DMFT calculations were used to obtain the statistical weight for different Co−3d

atomic states at T = 20, 300 and 700 K. The dependencies of these values on the Δ_{p-d} for different atomic states are shown in Fig.6. Our results indicated that the change in the relative position of ion and ligand levels can lead to the appearance of a complicated spin-state transition at any temperature in the given interval of Δ_{p-d}. The temperature variation shifts the transition region, preserving the relation between the statistical weights of atomic states. The transition occurs in a rather narrow range of the Δ_{p-d} parameter variation (less than 0.1 eV), which indicates a high sensitivity of the cobalt ion spin state to the relative position of the d- and p-states. These results are in good agreement with the previous reports [42–44, 59, 60]. We also found that the weights of $d^7\underline{L}$ states make a significant contribution to the total spin state, while the statistical weight of the intermediate d^6 state is about 10% and it almost remains constant through the spin-state transition. At the same time, the IS $d^7\underline{L}$ state [45] with S_{tot}=1 shows an increase of the statistical weight from 10 to 30% over the same region. This state arises from the transfer of an electron from the ligand p-state to d-state of the transition metal ion due to a strong hybridization. As a result, a hole and one unpaired electron are formed at the ligand p-level. The total spin of such configuration can be interpreted as S_{tot}=1 [61].

IV. DISCUSSION

Using a combination of three independent techniques, EXAFS, neutron and x-ray scattering measurements, we have determined the static and dynamic properties of Co-O bond in $LaCoO_3$, which underwent significant changes with the temperature. The temperature-dependence of these properties is a key to understanding the spin-state transitions in our samples. We begin our discussion by comparing the results of x-ray and neutron diffraction data for $LaCoO_3$ sample and reference sample of $LaGaO_3$. A striking difference between of $LaCoO_3$ sample from reference $LaGaO_3$ lies in an unusual increase of MSD_{Co-O} below 50 K, which was only observed in $LaCoO_3$ sample by neutron and x-ray scattering experiments [13]. Such behavior is an indication of the higher spin states of Co^{3+} ions below 50 K, which are absent in $LaGaO_3$ sample. This idea is further supported by the change of the slope of the isotropic ADP for Co at 50 K (Fig.4b). Next, we will argue that the spin state below 50 K is best described by a mixture of LS and HS. It is well documented that the

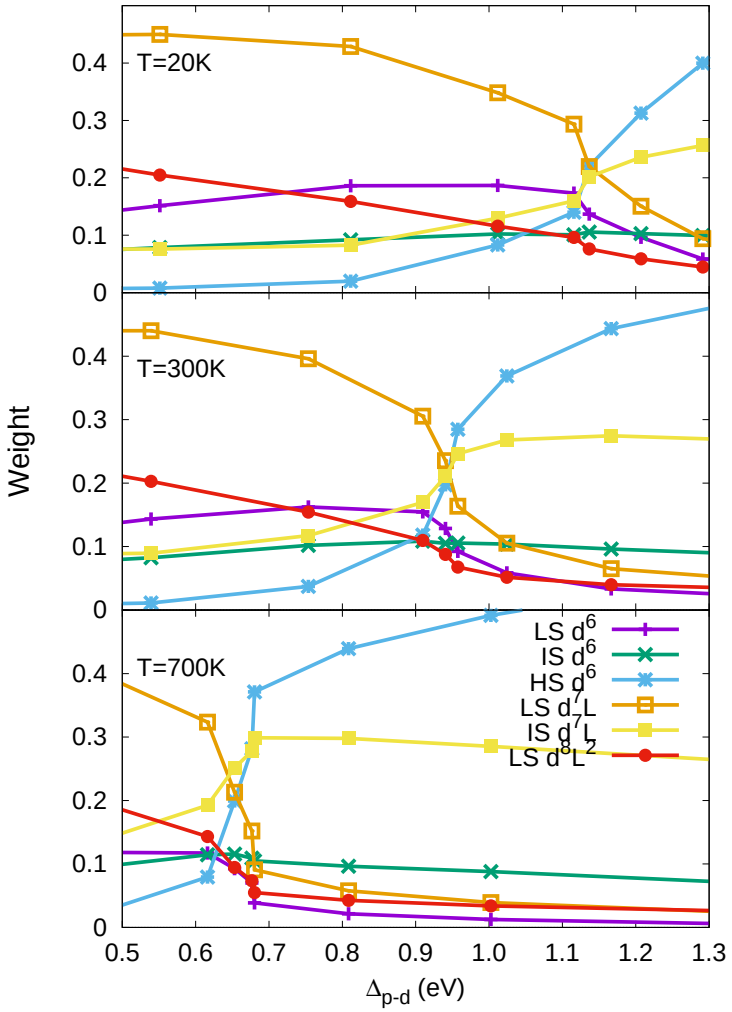

FIG. 6: The statistical weights of the dominant atomic configurations of the Co ions in $LaCoO_3$ as a function of Δ_{p-d} for the crystal structures at different temperatures.

ionic radius of the HS state (0.61 Å) is significantly larger than that for LS (0.54 Å) and IS (0.56 Å) states. Therefore, the mixture of LS and HS states leads to a significant strain that we observed in the x-ray data analysis (Fig.4a). The strain parameter decreases with the temperature and reaches its minimum value at about 150 K. We assigned this behavior (further confirmed by DMFT calculations) to the transition of the HS states presumably at the surface of powder crystallites into IS states, while the core of crystallites remains in the LS state. As the population of the HS states is being replaced by the IS states with the ionic radius similar to LS, the strain within the crystallites is effectively revealed at 150 K. Our conclusion is consistent with results of the single-crystal diffraction (Fig.3b). The

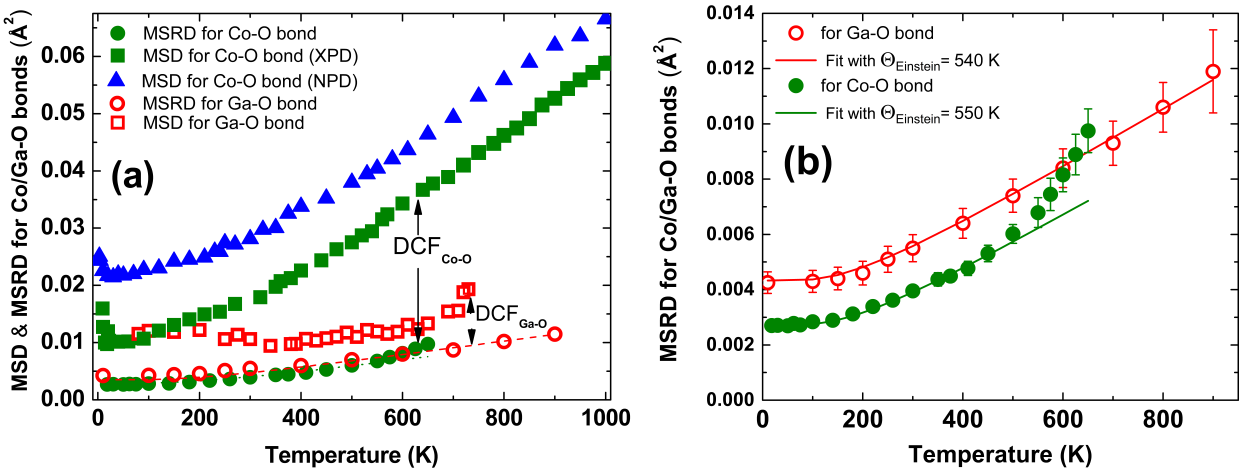

FIG. 7: (a) Temperature dependence of MSD obtained from XPD (■)/NPD (▲) and calculated $MSRD_{||}$ (•) for Co−O bond. Temperature dependence of MSD (□) and $MSRD_{||}$ (◯) calculated for Ga−O bond in $LaGaO_3$ sample. (b) Enlarged view of (a), showing $MSRD_{||}$ for Co−O (•) and Ga−O (◯) bonds. Solid lines are the fits to Einstein model.

largest ionic radius of the HS state explains why the difference between $U_{\perp}$ and $U_{||}$ above 600 K is larger than below 600 K. Consequentially, the difference between $< r_{Co-O} >$ and R_{Co-O} values (see Eq.1) is a result of the gradual spin-state transition of Co^{3+} ions from HS surface states into the highly-hybridized metallic IS states.

We further quantify the difference in spin-states for $LaCoO_3$ and $LaGaO_3$ samples, by plotting the temperature dependence of the displacement correlation function (DCF) for Co−O and Ga−O bonds in $LaCoO_3$ and $LaGaO_3$ samples, respectively (Fig.7a). The DCF describes the difference between uncorrelated MSD obtained by diffraction and correlated $MSRD_{||}$ obtained by EXAFS. It reflects the correlation in the atomic motion of Co/Ga and O atoms and defines the strength of the corresponding bond. The DCF_{Co-O} is gradually increasing with temperature in the $LaCoO_3$ sample, while the DCF_{Ga-O} in the $LaGaO_3$ sample is approximately constant up to $\sim$ 650 K. The weak temperature dependence of DCF_{Ga-O} is an indication of LS state of Ga^{3+} ions in this temperature range. In contrary, an increase of DCF_{Co-O} with the temperature can be associated with the gradual transition from the LS states into the higher spin states.

At higher temperatures, the considerable change of crystallographic parameters was observed at the metal-insulator transition (550 K). Fig.7b shows a change of the slope in the temperature dependence of the $MSRD_{||}$ of Co−O bond above 550 K, while no change of slope was observed for Ga−O bond. Both strain parameter (Fig.4a) and isotropic ADP for Co (Fig.4b) change the slope at metal-insulator transition. We ascribe all these effects to the increasing of HS states population, with the largest ionic radius as compared to the LS and IS states. In the frame of the proposed model, a minimal difference of the Co−O bond lengths obtained by XPD/NPD and EXAFS near 650 K in powder sample, can be associated with a gradual growth and saturation of the long-range IS domains with emerging fraction of the HS domains at around 550 - 600 K. The Co−O bond length obtained from EXAFS experiments shows a dip around 550 K (Fig.3a). At about the same temperature Co−O bond length begins to deviate from the linear slope, for both neutron and x-ray diffraction data. Taken together, it provides an evidence of the IS to HS state transition, which is consistent with previous electrical resistivity data [11].

It was previously shown that even in the case of the bulk crystal of $LaCoO_3$, its electronic structure cannot be properly described by a pure d^6 spin state at any temperatures [42, 43, 62, 63]. The correct description of the spin-state transition mechanism requires to take into account the charge and spin fluctuations arising from strong pd-hybridization and Coulomb correlations, which lead to the appearance of the charge-transfer multiplet states, in addition to the states with a formal valence of Co [44, 45]. Yaroslavtsev et al. [59] reported that the multiplet configuration of cobalt ions is very sensitive to the presence and properties of the surface. Hence, the perturbations of a local environment of Co ions gradually decrease when moving from the surface inwards the crystallite. In particular, it affects the relative position of O-p and Co-d levels, which in turn can affect the spin configuration of the cobalt ions. In order to study the effects of hybridization between O-2p and Co-3d orbitals on the spin-state transition we performed the electronic structure calculations using the DFT+DMFT approach and varied a distance between centers of the ligand p- and d-bands of the Co ions [31–34]. It was achieved by adding Δ_{p-d} parameter to the total energy functional during the DMFT self-consistency cycle.

We analyzed the dependence of the ionic radius of cobalt on Δ_{p-d} in the region of the

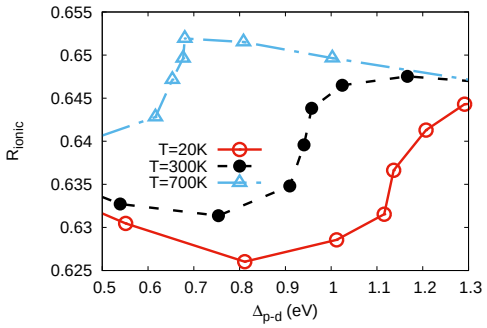

FIG. 8: (Color online) The ionic radius of Co in $LaCoO_3$ as a function of the Δ_{p-d} at 20, 300 and 700 K. Solid lines are guides for the eye.

spin-state transition. The ionic radius of a given Co atom was obtained by using the statistical weights of all atomic states consisting a resulting solution, as well as previously reported values [64] for the cobalt ions in the different spin-states. Figure 8 shows the dependence of the Co ionic radius on Δ_{p-d}. The non-linear dependence is due to the fact that the spin-state transition has a complex character and the resulting solution is a superposition of the several different atomic configurations. It can be seen that the dependence undergoes a sharp jump in the vicinity of the spin-state transition. From this we can conclude that even small changes in the ligand environment of the cobalt ion caused by the presence of a surface can dramatically change its magnetic configuration. Thus, for cobalt ions on the crystallite surface it becomes more energetically favorable to transition into a multiplet configuration, which is a superposition of states with a dominant contribution of the HS states. Conversely, for cobalt ions, which are at a sufficient distance from the surface, the probability of transition to the LS configuration will be higher. This conclusion agrees well with the experimental observations presented in this paper. The difference of the ionic radius between maximum value at 700 K and minimum value at 20 K is about 0.024 Å, which is in an excellent agreement with experimental value of 0.020 Å, obtained for Co−O bond in XPD and EXAFS measurements.

In our modeling, we had to apply a really laborious method to describe various spin transitions in our samples. It is a powerful tool for analyzing correlated systems and it is particularly suited for description of the temperature effects that play a crucial role in $LaCoO_3$ sample. The method is ab initio, which means that structural parameters (lattice

constants, symmetry group and atomic positions) were taken from the experimental data and used as an input for the simulations. Such approach is sufficient to effectively model the most important features of the electronic structure of crystalline solids. In the calculations, the exact surface structure was not modeled, but a qualitative interpretation is presented based on a change in the degree of hybridization between the ion and the ligand, depending on the closeness of the surface layer.

V. CONCLUSIONS

We have used a combination of high-resolution EXAFS at the Co and Ga K-edges, synchrotron x-ray and neutron powder diffraction on $LaCoO_3$ and $LaGaO_3$ samples and single-crystal neutron diffraction on $LaCoO_3$ sample to study spin-state and metal-insulator transitions of Co^{3+}. The sample $LaGaO_3$ was chosen as a reference, because it shows neither spin-state nor metal-insulator transitions. Our experimental results combined with theoretical calculations helped to elucidate the origin of the anomalous temperature dependence of Co-O bond lengths, DCF, strain parameter, and isotropic ADP for Co and O in the wide temperature range from 2 K up to 1000 K. The analysis of experimental data suggests that the Co ions are dominantly in the LS states at low temperatures, with a minority of the HS state presumably located at the surface of the powder crystallites. As the temperature increases from 5 K to 150 K, a gradual transformation of the surface HS states into highly-hybridized IS states takes place. At the same time, Co located in the inner part (core) of the crystallites remain in the LS state configuration up to 150 K. When the temperature is further increased up to 550 K, the gradual spin-state transition from the LS states into the IS states occurs. This is confirmed by our theoretical DFT+DMFT calculations. It was also found that a slight change in the degree of hybridization due to the proximity of the surface layer, can induce a spin-state transition at any temperature in the observed region. This scenario agrees well with recently published works [43, 59]. The experimental data obtained above 550 K can be well explained assuming a partial spin-state transition from configuration with dominant IS state into the configuration with prevailing HS state.

VI. ACKNOWLEDGMENTS

We are grateful to S. Lapidus for his help with the measurements at Advanced Photon Source. Measurements at SPring-8 were performed with the approval of the Japan Synchrotron Radiation Research Institute. Authors are indebted to V. Efimov for stimulating discussions and to D. Chernyshov (ESRF) for his help with diffraction experiments and data analysis and to A. Kuzmin for software creation to calculate $U_{\perp}$ and $U_{||}$ from anisotropic ADP. The results of theoretical part of the work including DFT+DMFT calculations were obtained within the state assignment of Minobrnauki of Russia (topic Electron No. AAAA-A18-118020190098-5). The calculations were performed using the Supercomputing center of IMM UrB RAS. Use of the Advanced Photon Source at Argonne National Laboratory was supported by the U. S. Department of Energy, Office of Science, Office of Basic Energy Sciences, under Contract Nr. DE-AC02-06CH11357. This work is based on experiments performed at the Swiss spallation neutron source SINQ, Paul Scherrer Institute, Villigen, Switzerland. The reported study was funded by RFBR according to the research project Nr. 17-302-50018-molnr. The authors would like to thank I. Bobrikov (JINR) for fruitful discussions. We thank N. Nandakumaran for the help with SEM measurements.

---

[1] P. G. Radaelli and S. W. Cheong, Phys. Rev. B **66**, 094408 (2002).

[2] G. Maris, Y. Ren, V. Volotchaev, C. Zobel, T. Lorenz, T. T. M. Palstra, Phys. Rev. B **67**, 224423 (2003).

[3] D. Louca, J.L. Sarrao, Phys. Rev. Lett. **91**, 155501 (2003).

[4] D. Phelan, D. Louca, S. Rosenkranz, S.-H. Lee, Y. Qiu, P. J. Chupas, R. Osborn, H. Zheng, J. F. Mitchell, J. R. D. Copley, J. L. Sarrao, Y. Moritomo Phys. Rev. Lett. **96** 027201 (2006).

[5] D.P. Kozlenko, N.O. Golosova, Z. Jirak, L.S. Dubrovinsky, B.N. Savenko, M.G. Tucker, Y. Le Godec, V.P. Glazkov, Phys. Rev. B **75**, 064422 (2007).

[6] N. Sundaram, Y. Jiang, I.E. Anderson, D.P. Belanger, C.H. Booth, F. Bridges, J.F. Mitchell, T. Proffen, H. Zheng, Phys. Rev. Lett. **102**, 026401 (2009).

[7] Y. Jiang, F. Bridges, N. Sundaram, D. P. Belanger, I. E. Anderson, J. F. Mitchell,H. Zheng, Phys. Rev. B **80**, 144423 (2009).

[8] K. Knìzek, Z. Jirak, J. Hejtmanek, M. Veverka, M. Marysko, G. Maris, T. T.M. PalstraEur.Phys. J. B **47** 213 (2005).

[9] T. Kyomen, Y. Asaka, and M. Itoh, Phys. Rev. B **71** 024418 (2005).

[10] R. Schmidt, J. Wu, C. Leighton, and I. Terry, Phys. Rev. B **79**, 125105 (2009).

[11] K. Asai, A. Yoneda, O. Yokokura, J. M. Tranquada, G. Shirane,K. Kohn, J. Phys. Soc. Jpn. **67**, 290 (1998).

[12] S. Yamaguchi, Y. Okimoto, H. Taniguchi, Y. Tokura, Phys. Rev. B **53**, R2926 (1996).

[13] C. Zobel, M. Kriener, D. Bruns, J. Baier, M. Grüninger, T. Lorenz, P. Reutler, A. Revcolevschi, Phys. Rev. B **66**, 020402(R) (2002).

[14] T. Kyomen, Y. Asaka, M. Itoh, Phys. Rev. B **67** 144424 (2003).

[15] P. M. Raccah and J. B. Goodenough, Phys. Rev. **155**, 932 (1967).

[16] M. A. Senaris-Rodriguez and J. B. Goodenough, J. Solid State Chem. **118**, 323 (1995).

[17] M. W. Haverkort, Z. Hu, J. C. Cezar, T. Burnus, H. Hartmann, M. Reuther, C. Zobel, T. Lorenz, A. Tanaka, N. B. Brookes, H. H. Hsieh, H.-J. Lin, C. T. Chen, L. H. Tjeng, Phys. Rev. Lett. **97**, 176405 (2006).

[18] A. Podlesnyak, S. Streule, J. Mesot, M. Medarde, E. Pomjakushina, K. Conder, A. Tanaka, M.W. Haverkort, D.I. Khomskii, Phys. Rev. Lett. **97**, 247208 (2006).

[19] S. Noguchi, S. Kawamata, K. Okuda, H. Nojiri, M. Motokawa, Phys. Rev. B **66**, 094404 (2002).

[20] K. Knzek, Z. Jirk, J. Hejtmnek, and P. Novk, J. Phys.: Condens.Matter **18**, 3285 (2006)

[21] S.K. Pandey, A. Kumar, S. Patil, V.R.R. Medicherla, R.S. Singh, K. Maiti, D. Prabhakaran, A. T. Boothroyd, and A. V. Pimpale, Phys. Rev. B **77**, 045123 (2008).

[22] M. Tachibana, T. Yoshida, H. Kawaji, T. Atake, and E. Takayama-Muromachi, Phys. Rev. B **77**, 094402 (2008).

[23] J. B. Goodenough, J. Alloys Compd. **262-263**, 1 (1997).

[24] L. Siurakshina, B. Paulus, V. Yushankhai, E. Sivachenko, Eur. Phys. J. B **74**, 5361 (2010).

[25] K. Knìžek, Z. Jiràk, J. Hejtmanek, P. Novàk, and Wei Ku, Phys. Rev. B **79**, 014430 (2009).

[26] K. Knìžek, J. Hejtmanek, Z. Jiràk, Petr Tomeš, P. Henry, and G. Andrè, Phys. Rev. B **79**, 134103 (2009).

[27] R. H. Potze, G. A. Sawatzky, M. Abbate, Phys. Rev. B **51**, 11501 (1995).

[28] S. Stølen, F. Grønvold, H. Brinks, T. Atake, H. Mori, Phys. Rev. B **55**, 14103 (1997).

[29] M.A. Korotin, S.Y. Ezhov, I.V. Solovyev, V.I. Anisimov, D.I. Khomskii, and G.A. Sawatzky, Phys. Rev. B **54**, 5309 (1996).

[30] V. Plakhty, P. Brown, B. Grenier, S. Shiryaev, S. Barilo, S. Gavrilov and E. Ressouche, J. Phys.: Condens. Matter **18** 35173525 (2006).

[31] W. Metzner, D. Vollhardt, Phys. Rev. Lett. **62**, 1066 (1989).

[32] A. Georges, G. Kotliar, W. Krauth, M. J. Rozenberg, Rev. Mod. Phys. **68**, 13 (1996).

[33] G. Kotliar, S. Y. Savrasov, K. Haule, V. S. Oudovenko, O. Parcollet, and C. A. Marianetti, Rev. Mod. Phys. **78**, 865 (2006).

[34] V. I. Anisimov, A. I. Poteryaev, M. A. Korotin, A. O. Anokhin, G. Kotliard, J. Phys.: Condens. Matter **9**, 7359 (1997).

[35] D. Prabhakaran, A. T. Boothroyd, F. R. Wondre, and T. J. Prior, J. Cryst. Growth **275**, e827 (2005).

[36] P. Fornasini, S. aBeccara, G. Dalba, R. Grisenti, A. Sanson, M. Vaccari, and F. Rocca, Phys. Rev. B **70**, 174301 (2004).

[37] P. Giannozzi et al., J. Phys.: Condens. Matter **21**, 395502 (2009).

[38] E. Gull, A. J. Millis, A. I. Lichtenstein, A. N. Rubtsov, M. Troyer, and P. Werner, Rev. Mod. Phys. **83**, 349 (2011).

[39] P. Werner, A. Comanac, L. de' Medici, M. Troyer, and A. J. Millis, Phys. Rev. Lett. **97**, 076405 (2006).

[40] P. Werner and A. J. Millis, Phys. Rev. B **74**, 155107 (2006).

[41] P. Werner and A. J. Millis, Phys. Rev. Lett. **99**, 126405 (2007).

[42] V. Krapek, P. Novak, J. Kunes, D. Novoselov, Dm. M. Korotin and V.I. Anisimov, Phys. Rev. B **86**, 195104 (2012).

[43] B. Chakrabarti, T. Birol, and K. Haule, Phys. Rev. Materials **1**, 064403 (2017).

[44] K. Tomiyasu, J. Okamoto, H.Y. Huang, Z.Y. Chen, E.P. Sinaga, W.B. Wu, Y.Y. Chu, A. Singh, R.-P. Wang, F.M.F. de Groot, A. Chainani, S. Ishihara, C.T. Chen, and D.J. Huang Phys. Rev. Lett. **119**, 196402 (2017).

[45] arxiv.org/abs/cond-mat/0101164

[46] A. Kuzmin, Physica B **208/209**, 175 (1995).

[47] J. Rodriguez-Carvajal, Physica B **192**, 55 (1993).

[48] V.V. Sikolenko, S.L. Molodtsov, M. Izquierdo, I.O. Troyanchuk, D. Karpinsky, S.I. Tiutiun-

nikov, E. Efimova, D. Prabhakaran, D. Novoselov, V. Efimova Physica B **536**, 597 (2018).

[49] A. Sanson, F. Rocca, G. Dalba, P. Fornasini, R. Grisenti, M. Dapiaggi, and G. Artioli, Phys. Rev B **73**, 214305 (2006).

[50] P. Fornasini, J. Phys.: Condens. Matter **13**, 7859 (2001).

[51] A. Herklotz, A. D. Rata, L. Schultz, and K. Dörr, Phys. Rev B **79**, 092409 (2009).

[52] K. Gupta and P. Mahadevan, Phys. Rev B **79**, 020406(R) (2009).

[53] V. V. Mehta, M. Liberati, F. J. Wong, R. V. Chopdekar, E. Arenholz and Y. Suzuki, J. Appl. Phys. **105**, 07E503 (2009).

[54] D. Fuchs, E. Arac, C. Pinta, S. Schuppler, R. Schneider and H. v. Löhneysen, Phys. Rev B **77**, 014434 (2008).

[55] W. S. Choi, J.-H. Kwon, H. Jeen, J. E. Hamann-Borrero, A. Radi, S. Macke, R. Sutarto, F. He, G. A. Sawatzky, V. Hinkov, M. Kim, H. N. Lee, Nano Lett. **12**, 4966 (2012).

[56] Y. Liu, K. Ma, Y. Yu, Surf Interface Anal. **49**, 1160 (2017).

[57] I. Fita, D. Mogilyansky, V. Markovich, R. Puzniak, A. Wisniewski, L. Titelman, L. Vradman, M. Herskowitz, V.N. Varyukhin, G. Gorodetsky, J. of Non-Cryst. Solids **354**, 5204 (2008).

[58] G. Beni and P. M. Platzman, Phys. Rev. B **14**, 1514 (1976).

[59] A. A. Yaroslavtsev, M. Izquierdo, R. Carley, M. E. Davila, A. A. Unal, F. Kronast, A. Lichtenstein, A. Scherz, and S. L. Molodtsov Phys. Rev. B **93**, 155137 (2016).

[60] M. Karolak, M. Izquierdo, S.L. Molodtsov, and A.I. LichtensteinPhys. Rev. Lett. **115**, 046401 (2015).

[61] M. V. Mostovoy and D. I. Khomskii, Phys. Rev. Lett. **92**, 167201 (2004),

[62] P. Augustinsky, V. Krapek, J. Kunes, Phys. Rev. Lett. **110**, 267204 (2013).

[63] G. Zhang, E. Gorelov, E. Koch, and E. Pavarini, Phys. Rev. B **86**, 184413 (2012).

[64] R.D. Shannon, Acta Cryst. **32**, 751 (1976); Asai K et al. Phys. Rev. B **40**, 10982 (1989); Itoth M et.al J. Phys. Soc Jpn. **64** 3967 (1995).